Accepted Manuscript

A semi-analytical model for predicting stress evolution in multilayer coating systems during thermal cycling

Biao Li , Xueling Fan , Kun Zhou , Tiejun Wang

PII: S0020-7403(17)31822-2
DOI: 10.1016/j.ijmecsci.2017.11.010
Reference: MS 4026

To appear in: *International Journal of Mechanical Sciences*

Received date: 5 July 2017
Revised date: 19 October 2017
Accepted date: 7 November 2017

Please cite this article as: Biao Li , Xueling Fan , Kun Zhou , Tiejun Wang , A semi-analytical model for predicting stress evolution in multilayer coating systems during thermal cycling, *International Journal of Mechanical Sciences* (2017), doi: 10.1016/j.ijmecsci.2017.11.010

This is a PDF file of an unedited manuscript that has been accepted for publication. As a service to our customers we are providing this early version of the manuscript. The manuscript will undergo copyediting, typesetting, and review of the resulting proof before it is published in its final form. Please note that during the production process errors may be discovered which could affect the content, and all legal disclaimers that apply to the journal pertain.

ACCEPTED MANUSCRIPT

Highlights

- A semi-analytical model is proposed to predict stress evolution in coating systems.
- Thermal gradient, oxide growth and creep relaxation are considered in the model.
- Creep plays key role in determining stress evolution during thermal cycling.
- Creep in the oxide is beneficial to the durability of the coating system.

ACCEPTED MANUSCRIPT

ACCEPTED MANUSCRIPT

A semi-analytical model for predicting stress evolution in multilayer coating systems during thermal cycling

Biao Li[a, b], Xueling Fan[a,*], Kun Zhou[b], Tiejun Wang[a,*]

[a] *State Key Laboratory for Strength and Vibration of Mechanical Structures, School of Aerospace Engineering, Xi'an Jiaotong University, Xi'an 710049, China*

[b] *School of Mechanical and Aerospace Engineering, Nanyang Technological University, Singapore 639798, Singapore*

Abstract

A semi-analytical model is developed to predict the stress evolution within a multilayer coating system during cyclic thermal loading. This model takes into account the temperature gradient across the thickness of the system, which is the common thermal conditions of the high-temperature protective coatings. The creep deformation and the oxide scale growth processes at the elevated temperature are considered in the theoretical framework. The cases of thermal barrier coatings are analyzed, and finite element analysis is performed for comparisons. The results show that the stress and creep strain fields solved by the semi-analytical method are consistent with the finite element predictions, which confirms the validity of the proposed model. The effects of creep in the system on the stresses and curvature evolutions are discussed. It is found that the large creep rates in the coatings or substrate could facilitate the stress relaxation processes in both of them, whereas the stress evolutions in the oxide scale are virtually unaffected. The curvature of the system may reverse from the concave to convex shape during the thermal cycling when the fast creep relaxations occur in the coatings. Furthermore, the creep deformations in the oxide scale provide benefits in relaxing the huge growth stresses so that the better durability of the system could be obtained.

Keywords: Stress evolution; Multilayer coating system; Thermal cycling; Creep relaxation; Oxidation

* Corresponding author:
Tel.: +86-29-82667864, Fax: +86-29-82669044
E-mail: fanxueling@mail.xjtu.edu.cn (X.L. Fan); wangtj@mail.xjtu.edu.cn (T.J. Wang)

ACCEPTED MANUSCRIPT

1. Introduction

Multilayer coating systems are widely used in the industry to provide protections for structural components against harsh environments [1-9]. For example, thermal barrier coatings (TBCs) are deposited on the superalloy substrate of gas turbine blades to provide the thermal and oxidation protections against high-temperature gas [4-6] and environmental barrier coatings (EBCs) are applied to protect SiC/SiC composites from high-temperature water vapor [7-9]. Such coating systems usually undergo cyclic thermal loading by experiencing periodic temperature change in a wide range. The thermal cycling inevitably introduces stresses into the coating layers because of the imposed non-uniform temperature fields and/or the thermal expansion mismatches among the layers. As the operation period extends, the stresses develop due to processes occurring in the high-temperature environment, such as the creep relaxation, oxidation, sintering, and phase transformation. Failure of the coatings takes place when the stresses evolve to some extents. The high compressive in-plane stresses may lead to buckling delamination of the coatings, and the tensile stresses could induce the onset and growth of surface cracks and interface cracks [10-15]. Therefore, understanding the stress evolutions during the thermal cycling is important to estimate the reliability and durability of the coating system.

The stress evolutions in the coating system are affected by the interactions among various factors associated with the thermal cycling, of which the thermal conditions, oxide scale growth, and creep deformations play the important roles [16-18]. During the cycling, the top and bottom surfaces of the system usually operate under different thermal conditions, and a thermal gradient is formed in the through-thickness direction of the system, e.g., the temperature gradient in the TBCs on the turbine blade is up to 300℃[4]. The thermal gradient induces the non-uniform expansions of a layer so that its stress distribution is intrinsically non-uniform. In such case, the stress difference at the interface of two adjacent layers may be enhanced when compared with the ones of uniform temperature field, which might lead to premature delamination of the coatings. Moreover, a thin layer of oxide scale could form and

ACCEPTED MANUSCRIPT

grow between the coatings and substrate at elevated temperature due to the oxidation of the substrate, e.g., the formed Al_2O_3 layer in the TBCs and the SiO_2 layer in the SiC-based EBCs [7, 16]. This growing oxide affects the stress evolutions in the system and usually induces the degradation of adherence strength of the adjacent layers. Cracking is often observed within or around the oxide [19]. Furthermore, viscous flows can be significant when the coatings are exposed to the high temperature [20-22]. Creep relaxation gives rise to the accumulations of inelastic strains and the redistributions of stresses. It further affects the residual stress fields when the coatings are cooled down.

Accurate predictions of stress evolutions in the coating system should account for the aforementioned important factors of thermal gradient condition, oxide scale growth, and creep relaxation. It is desirable to have a comprehensive analytical model that can efficiently predict the stress evolutions during the thermal cycling. However, there are few analytical works that attempted to address this issue. Most of the previous investigations focused on the analytical analysis of thermoelastic stresses in the linear elastic multilayer film/substrate system [23-27]. For instance, Hsueh [26] developed an exact closed-form solution to evaluate the thermal stresses in elastic multilayer systems, in which only three boundary conditions are required to solve the stress fields regardless of the number of layers in the system. Hsueh's method has been widely employed to analyze residual stresses within various systems, such as thermal barrier coatings, multilayer films/substrate system, and multilayer beams [28-31]. Nonetheless, their works are limited to the cases of linear elastic system, in which the factors of creep relaxation, oxide scale growth, and temperature gradient are not considered. Though a few works devoted to the issues of stress relaxations in the multilayer films [32-34], a uniform temperature change with a single heating or cooling process is commonly imposed and the growth of oxide scale is not taken into account. Hence, the roles of oxide growth and creep deformations on the stress evolutions within multilayer coating system during thermal cycling have not yet been well understood.

This work aims to present a semi-analytical model to evaluate the stress evolution in the

multilayer coating system during the thermal cycling. The thermal gradient condition, oxide scale growth, and creep relaxation are taken into account in the theoretical framework. The model is derived in Section 2. In Section 3, comparisons between the semi-analytical and finite element predictions are made to validate the proposed model. In Section 4, the effects of creep in the layers on the stress evolutions are discussed. Conclusions are made in Section 5.

2. Model development

2.1 Problem description

A typical multilayer coating system is schematically shown in Fig. 1(a). The n layers of coatings are bonded sequentially to a substrate and a thin oxide scale is formed between the substrate and the first coating layer. The interfaces between the layers are considered to be flat and perfectly bonded. The thicknesses of the substrate, oxide scale, and individual coating are denoted as h_s, h_g and h_i (i=1, 2,..., n), respectively. The coordinate axis x is located at the interface between the layer 1 and the oxide, and the z-axis is along the thickness direction of the system. The z coordinates of the upper and lower interfaces of layer i are, respectively, denoted as z_i and z_{i-1} ($z_0 = 0$), in which a relation of $h_i = z_i - z_{i-1}$ is derived.

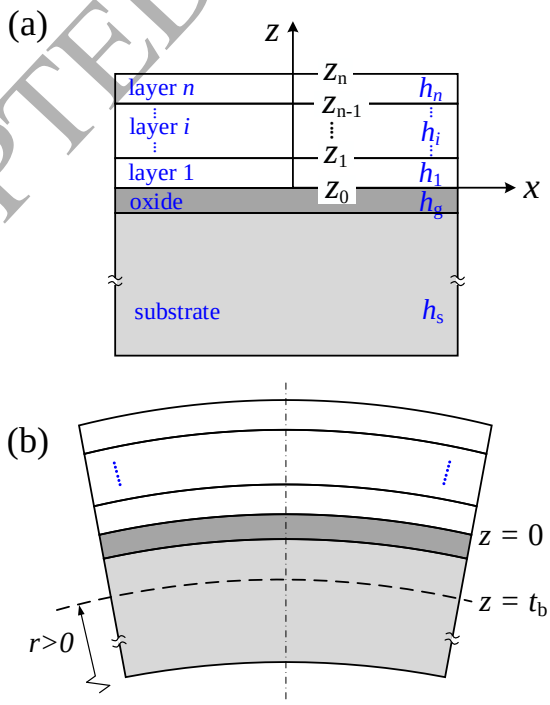

Fig. 1. Schematic diagrams showing: (a) a multilayer coating system ($h_i = z_i - z_{i-1}$ and $z_0 = 0$)

ACCEPTED MANUSCRIPT

and (b) bending induced by the asymmetric stresses.

When the in-plane dimension (*x*-*y* plane) of the multilayer coating system is much larger than its thickness, the system curves spherically under thermal loading and an equal biaxial in-plane stress state is formed. However, when the system is assumed to be a strip, the stresses in the width direction (σ_y herein) vanishes and the system is in a uniaxial stress state. In the most realistic geometrical condition, the coating system has a large planar geometry. Therefore, the equal biaxial in-plane stress state ($\sigma_x = \sigma_y$) is assumed in the model. In addition, all layers are considered to be isotropic.

The imposed cyclic thermal loading and the corresponding deformation are qualitatively described as follows. For an initially stress-free system, its top and bottom surfaces are, respectively, heated up to the elevated temperatures T_t^{max} and T_b^{max} (with $T_t^{max} \geq T_b^{max}$), as depicted in Fig. 2(a). The thermal gradient is introduced in the through-thickness direction of the system. In this process, the arising asymmetric thermal stresses induce the bending of the system and a bending curvature is formed. Then, the thermal gradient is held for a period of time, during which the creep deformations of the layers occur to induce the stress relaxations. As the holding time extends, the stress fields are redistributed and thus the bending curvature varies, as illustrated in Fig. 2(b). The growth of oxide scale may contribute to such redistributions and variations. After that, the system is steadily cooled down to the ambient temperature. The curvature may change again and some stresses and deformations remain in the system. Above thermal loading process may be periodically imposed and the stresses and curvature vary with the cycling.

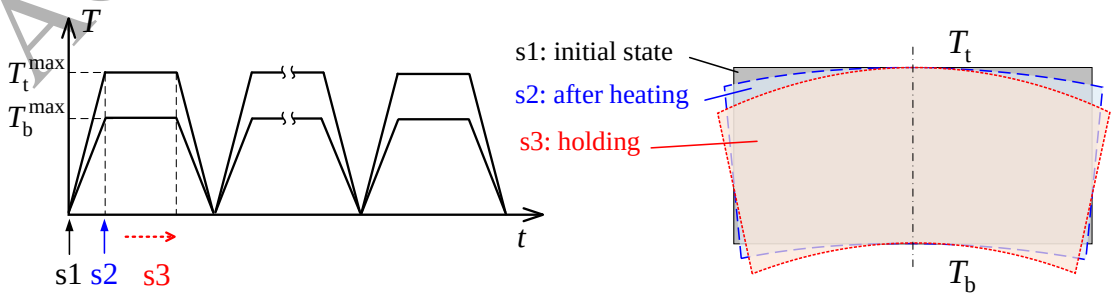

(a) (b)

ACCEPTED MANUSCRIPT

Fig. 2. Schematic diagrams showing: (a) variations of temperature T with time t and (b) variations of curvature of the system with the thermal cycling.

2.2 Temperature fields

In the analysis of temperature fields, three assumptions are made for simplification: (1) the heat conduction during the entire thermal cycles is steady; (2) no thermal convection or radiation occurs; (3) no interfacial thermal resistance exists.

For the multilayer coating system shown in Fig. 1(a), the heat flux density, q, can be written as follows:

$$q = -\frac{T_{\mathrm{t}}(t) - T_{\mathrm{b}}(t)}{R_{\mathrm{total}}} \quad \text{, with} \quad R_{\mathrm{total}} = \sum_{i=1}^{n} \frac{h_i}{\lambda_i} + \frac{h_{\mathrm{g}}}{\lambda_{\mathrm{g}}} + \frac{h_{\mathrm{s}}}{\lambda_{\mathrm{s}}}, \tag{1}$$

where $T_{\mathrm{t}}(t)$ and $T_{\mathrm{b}}(t)$ are the imposed temperatures as functions of time t at the top surface and bottom surface of the system, respectively. R_{total} is the thermal resistance of the system, n the numbers of coating layers, and λ the thermal conductivity. The subscripts i, g and s denote the i-th layer of the coatings, oxide scale and substrate, respectively. It is assumed that the thermal conductivities are constant during the cycling.

Note that the net heat flux at any material point is zero. Thus, the heat flux density q can also be written based on a given location z as follows:

$$q = \begin{cases} -\dfrac{T_{\mathrm{t}}(t) - T(z,t)}{\displaystyle\sum_{j=i+1}^{n} \frac{h_j}{\lambda_j} + \frac{z_i - z}{\lambda_i}}, & z_{i-1} \le z \le z_i \\ -\dfrac{T_{\mathrm{t}}(t) - T(z,t)}{\displaystyle\sum_{i=1}^{n} \frac{h_i}{\lambda_i} - \frac{z}{\lambda_{\mathrm{g}}}}, & -h_{\mathrm{g}} \le z \le 0 \\ -\dfrac{T_{\mathrm{t}}(t) - T(z,t)}{\displaystyle\sum_{i=1}^{n} \frac{h_i}{\lambda_i} + \frac{h_{\mathrm{g}}}{\lambda_{\mathrm{g}}} + \frac{-h_{\mathrm{g}} - z}{\lambda_{\mathrm{s}}}}, & -\left(h_{\mathrm{s}} + h_{\mathrm{g}}\right) \le z \le -h_{\mathrm{g}} \end{cases}, \tag{2}$$

where $T(z, t)$ is the temperature at the location z.

Using Eqs. (1) and (2), the solutions of temperature distribution in the z-direction at any

instant of the thermal cycles are given as follows:

$$T(z,t)=\begin{cases} T_{\mathrm{t}}(t)-\dfrac{T_{\mathrm{t}}(t)-T_{\mathrm{b}}(t)}{R_{\mathrm{total}}}\left(\displaystyle\sum_{j=i+1}^{n}\frac{h_j}{\lambda_j}+\frac{z_i-z}{\lambda_i}\right), & z_{i-1}\le z<z_i \\ T_{\mathrm{t}}(t)-\dfrac{T_{\mathrm{t}}(t)-T_{\mathrm{b}}(t)}{R_{\mathrm{total}}}\left(\displaystyle\sum_{i=1}^{n}\frac{h_i}{\lambda_i}-\frac{z}{\lambda_{\mathrm{g}}}\right), & -h_{\mathrm{g}}\le z<0 \\ T_{\mathrm{t}}(t)-\dfrac{T_{\mathrm{t}}(t)-T_{\mathrm{b}}(t)}{R_{\mathrm{total}}}\left(\displaystyle\sum_{i=1}^{n}\frac{h_i}{\lambda_i}+\frac{h_{\mathrm{g}}}{\lambda_{\mathrm{g}}}+\frac{-h_{\mathrm{g}}-z}{\lambda_{\mathrm{s}}}\right), & -\left(h_{\mathrm{s}}+h_{\mathrm{g}}\right)\le z<-h_{\mathrm{g}} \end{cases} . \quad (3)$$

2.3 Stress fields

The total strain in the system can be decomposed into a uniform component and a bending component [26]. The concept of bending axis is used, which is defined as a reference plane in the system where the bending strain is zero. Hence, the total strain is expressed as

$$\varepsilon(z,t)=c(t)+\frac{z-t_{\mathrm{b}}(t)}{r(t)} \quad \text{, with } -\left(h_{\mathrm{s}}+h_{\mathrm{g}}\right)\le z\le z_n\text{,} \quad (4)$$

where $\varepsilon(z, t)$ is the total strain as functions of coordinate z and time t, $c(t)$ the uniform strain component, $z = t_{\mathrm{b}}(t)$ the position of bending axis, and $r(t)$ the radius of curvature of the system at the bending axis position. The radius is defined to be positive ($r(t) > 0$) when the system bends in a convex shape (Fig. 1(b)), and vice versa. Note that the bending axis differs from the conventional neutral axis in classical beam bending theory, which is defined as the axis where the normal stress is zero.

The general formulations for the stresses in the x-axis direction at any instant of the thermal cycles can be written as follows:

$$\begin{cases} \sigma_i(z,t)=E_i\left[\varepsilon(z,t)-\alpha_i\Delta T(z,t)-\varepsilon_{\mathrm{c}}(z,t)\right], & z_{i-1}\le z\le z_i \\ \sigma_{\mathrm{g}}(z,t)=E_{\mathrm{g}}\left[\varepsilon(z,t)-\alpha_{\mathrm{g}}\Delta T(z,t)-\varepsilon_{\mathrm{c}}(z,t)-\varepsilon_{\mathrm{gl}}(t)\right], & -h_{\mathrm{g}}\le z\le 0 \\ \sigma_{\mathrm{s}}(z,t)=E_{\mathrm{s}}\left[\varepsilon(z,t)-\alpha_{\mathrm{s}}\Delta T(z,t)-\varepsilon_{\mathrm{c}}(z,t)\right], & -\left(h_{\mathrm{s}}+h_{\mathrm{g}}\right)\le z\le -h_{\mathrm{g}} \end{cases} , \quad (5)$$

where σ, E and α are stress in the x-axis direction, biaxial modulus, and coefficient of thermal expansion (CTE). $E=E^*/(1-\nu)$, where E^* is the Young's modulus and ν is the Poisson's ratio. $\Delta T(z, t)$ is temperature change related to the initial ambient temperature T_0, $\Delta T(z, t)=T(z, t)-T_0$.

ACCEPTED MANUSCRIPT

ε_c is the accumulated creep strain and ε_{gl} is the growth strain induced by the lateral growth of the oxide, both of which are initially zero.

It is seen that the calculations of stresses depend on the solutions of $c(t)$, $r(t)$ and $t_b(t)$. Three boundary conditions are used to solve these variables.

(i) The resultant force due to the uniform strain component is zero, which is written as

$$\begin{aligned}\int_{-(h_s+h_g)}^{-h_g} E_s\left[c(t)-\alpha_s\Delta T(z,t)-\varepsilon_c(z,t)\right]\mathrm{d}z+\sum_{i=1}^{n}\int_{z_{i-1}}^{z_i} E_i\left[c(t)-\alpha_i\Delta T(z,t)-\varepsilon_c(z,t)\right]\mathrm{d}z \\ +\int_{-h_g}^{0} E_g\left[c(t)-\alpha_g\Delta T(z,t)-\varepsilon_c(z,t)-\varepsilon_{gl}(t)\right]\mathrm{d}z=0\end{aligned}. \quad (6)$$

(ii) The resultant force due to the bending strain component is zero, which is written as

$$\int_{-(h_s+h_g)}^{-h_g} E_s\frac{z-t_b(t)}{r(t)}\mathrm{d}z+\int_{-h_g}^{0} E_g\frac{z-t_b(t)}{r(t)}\mathrm{d}z+\sum_{i=1}^{n}\int_{z_{i-1}}^{z_i} E_i\frac{z-t_b(t)}{r(t)}\mathrm{d}z=0. \quad (7)$$

(iii) The sum of the bending moment with respect to bending axis is zero, which is written as

$$\begin{aligned}\int_{-(h_s+h_g)}^{-h_g}\sigma_s(z,t)\left[z-t_b(t)\right]\mathrm{d}z+\int_{-h_g}^{0}\sigma_g(z,t)\left[z-t_b(t)\right]\mathrm{d}z \\ +\sum_{i=1}^{n}\int_{z_{i-1}}^{z_i}\sigma_i(z,t)\left[z-t_b(t)\right]\mathrm{d}z=0\end{aligned}. \quad (8)$$

To simplify the expressions, the biaxial modulus and CTE in the layers are, respectively, written in the forms of piecewise functions as $E(z)$ and $\alpha(z)$, which are

$$E(z)=\begin{cases}E_i, & z_{i-1}\le z\le z_i\\ E_g, & -h_g\le z\le 0\\ E_s, & -(h_s+h_g)\le z\le -h_g\end{cases} \text{ and } \alpha(z)=\begin{cases}\alpha_i, & z_{i-1}\le z\le z_i\\ \alpha_g, & -h_g\le z\le 0\\ \alpha_s, & -(h_s+h_g)\le z\le -h_g\end{cases}. \quad (9)$$

By solving the Eqs. (6)-(8), one obtains

$$c(t)=\frac{\int_{-(h_s+h_g)}^{z_n} E(z)\alpha(z)\Delta T(z,t)\mathrm{d}z+E_g\varepsilon_{gl}(t)h_g+\int_{-(h_s+h_g)}^{z_n} E(z)\varepsilon_c(z,t)\mathrm{d}z}{E_sh_s+E_gh_g+\sum_{i=1}^{n}E_ih_i}, \quad (10)$$

$$t_b(t)=\frac{E_s\left(h_g^{\,2}-(h_s+h_g)^2\right)-E_gh_g^{\,2}+\sum_{i=1}^{n}E_i\left(z_i^2-z_{i-1}^2\right)}{2\left(E_sh_s+E_gh_g+\sum_{i=1}^{n}E_ih_i\right)}, \quad (11)$$

ACCEPTED MANUSCRIPT

$$r(t)=\frac{a_{11}+a_{12}+a_{13}}{b_{11}+b_{12}+b_{13}}, \tag{12}$$

where

$$a_{11}=\left(E_{\mathrm{s}}h_{\mathrm{s}}+E_{\mathrm{g}}h_{\mathrm{g}}+\sum_{i=1}^{n}E_{i}h_{i}\right)t_{\mathrm{b}}(t)^{2}, \tag{13}$$

$$a_{12}=E_{\mathrm{s}}t_{\mathrm{b}}(t)\left(h_{\mathrm{s}}{}^{2}+2h_{\mathrm{s}}h_{\mathrm{g}}\right)+E_{\mathrm{g}}t_{\mathrm{b}}(t)h_{\mathrm{g}}{}^{2}+\sum_{i=1}^{n}E_{i}t_{\mathrm{b}}(t)\left(z_{i-1}{}^{2}-z_{i}{}^{2}\right), \tag{14}$$

$$a_{13}=\frac{1}{3}E_{\mathrm{s}}\left[\left(h_{\mathrm{s}}+h_{\mathrm{g}}\right)^{3}-h_{\mathrm{g}}{}^{3}\right]+\frac{1}{3}E_{\mathrm{g}}h_{\mathrm{g}}{}^{3}+\frac{1}{3}\sum_{i=1}^{n}E_{i}\left(z_{i}{}^{3}-z_{i-1}{}^{3}\right), \tag{15}$$

$$b_{11}=-\frac{h_{\mathrm{g}}{}^{2}}{2}E_{\mathrm{g}}\varepsilon_{\mathrm{gl}}(t)-E_{\mathrm{g}}h_{\mathrm{g}}t_{\mathrm{b}}\varepsilon_{\mathrm{gl}}+\left(E_{\mathrm{s}}h_{\mathrm{s}}+E_{\mathrm{g}}h_{\mathrm{g}}+\sum_{i=1}^{n}E_{i}h_{i}\right)t_{\mathrm{b}}(t)c(t), \tag{16}$$

$$b_{12}=\frac{c(t)}{2}\left[E_{\mathrm{s}}\left(\left(h_{\mathrm{s}}+h_{\mathrm{g}}\right)^{2}-h_{\mathrm{g}}{}^{2}\right)+E_{\mathrm{g}}h_{\mathrm{g}}{}^{2}+\sum_{i=1}^{n}E_{i}\left(z_{i-1}{}^{2}-z_{i}{}^{2}\right)\right], \tag{17}$$

$$b_{13}=\int_{-\left(h_{\mathrm{s}}+h_{\mathrm{g}}\right)}^{z_{n}}E(z)\alpha(z)\Delta T(z,t)\left[z-t_{\mathrm{b}}(t)\right]\mathrm{d}z+\int_{-\left(h_{\mathrm{s}}+h_{\mathrm{g}}\right)}^{z_{n}}E(z)\varepsilon_{\mathrm{c}}(z,t)\left[z-t_{\mathrm{b}}(t)\right]\mathrm{d}z\,. \tag{18}$$

Due to the difficulty in deriving the closed-form integrations of time-dependent creep strains, the compound Cotes integration formulation is used to numerically calculate the integrations associated with ε_{c}. The detailed solutions of Eqs. (10) and (18) are given in Appendixes A and B. By substituting Eqs. (10)-(12) into Eqs. (4) and (5), the stress and strain distributions in the system could be solved. The iterative approach is used to calculate the stress evolution during the thermal cycling. It should be pointed out that the multilayer coating system is assumed to be initially stress-free at the initial instant t = 0. For t > 0, residual stresses would arise at end of the cooling stage of a thermal cycle due to the creep relaxation occurring at the high-temperature holding period. In the model, the residual stresses in a thermal cycle are inherently taken as the initial stresses for the next cycle. Therefore, the effect of residual stresses during the cycling has been included in Eqs. (4) and (5).

In addition, the oxide scale gradually grows both in the thickness and lateral directions so that the h_{g} and $\varepsilon_{\mathrm{gl}}$ are monotonically increasing. In some cases, modulus of the oxide scale

may be very large, e.g., the one in TBCs is about 400 GPa. Hence, according to the above solutions, the oxidation process may significantly affect the stress evolutions as well as the variations of curvature of the system. Particularly, the location of the bending axis would vary with the thickening oxide. This finding differs from the conclusions made in previous investigations for multilayer system without the oxide scale, who found that the bending axis keeps the same location during the loading history [32-34]. Moreover, above formulations are able to reduce to the conventional case for evaluating the thermoelastic stresses in the linear elastic multilayers film/substrate system when the creep strains and growth strains are ignored and uniform temperature field is imposed, as given in [26].

2.4 Creep deformation

Steady-state creep deformation is assumed during the cycling. The Norton's power law creep relation is employed, which is given as follows:

$$\dot{\varepsilon}_{\mathrm{c}}\left(z,t\right)=\begin{cases}\mathrm{sign}\left[\sigma_i\left(z,t\right)\right]B_i\sigma_i\left(z,t\right)^{n_i} & z_{i-1}\le z\le z_i\\ \mathrm{sign}\left[\sigma_{\mathrm{g}}\left(z,t\right)\right]B_{\mathrm{g}}\sigma_{\mathrm{g}}\left(z,t\right)^{n_{\mathrm{g}}} & -h_{\mathrm{g}}\le z\le 0\\ \mathrm{sign}\left[\sigma_{\mathrm{s}}\left(z,t\right)\right]B_{\mathrm{s}}\sigma_{\mathrm{s}}\left(z,t\right)^{n_{\mathrm{s}}} & -\left(h_{\mathrm{s}}+h_{\mathrm{g}}\right)\le z\le -h_{\mathrm{g}}\end{cases}, \tag{19}$$

where $\mathrm{sign}\left[\sigma\left(z,t\right)\right]=\sigma\left(z,t\right)/\left|\sigma\left(z,t\right)\right|$ is the sign function, $\dot{\varepsilon}_{\mathrm{c}}\left(z,t\right)$ the creep strain rate, B the creep prefactor, and n the creep exponent.

During the heating and cooling periods of the cycling, the time for the temperature held in the range where the creep relaxation can occur is relatively short. Therefore, creep strains are assumed to accumulate only during the high temperature holding period. At any instant of the cycling, the creep strain is updated as

$$\begin{cases}\varepsilon_{\mathrm{c}}\left(z,t+\Delta t\right)=\varepsilon_{\mathrm{c}}\left(z,t\right)+\dot{\varepsilon}_{\mathrm{c}}\left(z,t\right)\Delta\tau\\ \varepsilon_{\mathrm{c}}\left(z,0\right)=0\end{cases}, \tag{20}$$

where Δt is the increment of total time and $\Delta\tau$ is the increment of holding time. It can be expressed as

$$\Delta\tau = \begin{cases} \Delta t, & \text{during the high-temperature holding period} \\ 0, & \text{during the heating and cooling processes} \end{cases}. \tag{21}$$

2.5 Growth of oxide scale

During the high-temperature exposure, the oxygen diffusing inward reacts with the substrate at the oxide scale/substrate interface to form the new oxide, which induces the oxide thickening, as depicted in Fig. 3. In the same process, the reaction occurs at the grain boundaries of the oxide to cause the lateral growth. In this work, the oxidation is assumed to occur only at the high-temperature holding period, which is the same reason for creep relaxation mentioned above.

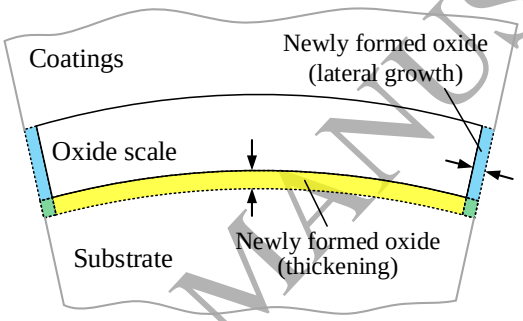

Fig. 3. Schematic diagram showing the growth of oxide scale both in the thickness and lateral directions.

The variations of oxide thickness during the high-temperature exposure could be determined by the experimental observations, and it is usually described by an oxidation kinetics curve. The thickness of oxide is defined as a function of its temperature and the high-temperature holding time, which is expressed as

$$h_{\mathrm{g}} = \left[k_{\mathrm{op}} \tau(t) \exp\left(-\frac{Q}{RT} \right) \right]^{m_{\mathrm{g}}} + h_{\mathrm{g}}^{0}, \tag{22}$$

where h_{g}^{0} is the initial thickness of the oxide, T the temperature of the oxide, R the gas constant, Q the system specific activation energy, m_{g} the exponent, and k_{op} the experimentally determined fitting parameter. The $\tau(t)$ is the accumulation of holding time, which is $\tau(t+\Delta t)= \tau(t)+ \Delta\tau$.

The growth strain rate of the oxide in the thickness direction, $\dot{\varepsilon}_{\mathrm{gt}}$, is formulated as

$$\dot{\varepsilon}_{\mathrm{gt}}(t)=\frac{1}{h_{\mathrm{g}}^{0}}\frac{\mathrm{d}\left(h_{\mathrm{g}}-h_{\mathrm{g}}^{0}\right)}{\mathrm{d}\tau}=\frac{m_{\mathrm{g}}}{h_{\mathrm{g}}^{0}}\left[k_{\mathrm{op}}\exp\left(-\frac{Q}{RT}\right)\right]^{m_{\mathrm{g}}}\tau(t)^{m_{\mathrm{g}}-1}. \tag{23}$$

The lateral growth strain rate, $\dot{\varepsilon}_{\mathrm{gl}}(t)$, is defined to be proportional to $\dot{\varepsilon}_{\mathrm{gt}}(t)$, which is

$$\eta_{\mathrm{g}}=\frac{\dot{\varepsilon}_{\mathrm{gl}}(t)}{\dot{\varepsilon}_{\mathrm{gt}}(t)}, \tag{24}$$

where η_{g} is the ratio of growth strain rates in the lateral direction to one in the thickness direction. Thus, the growth strain is derived as

$$\begin{cases}\varepsilon_{\mathrm{gt}}(t+\Delta t)=\varepsilon_{\mathrm{gt}}(t)+\dot{\varepsilon}_{\mathrm{gt}}(t)\Delta\tau\\ \varepsilon_{\mathrm{gl}}(t+\Delta t)=\varepsilon_{\mathrm{gl}}(t)+\dot{\varepsilon}_{\mathrm{gl}}(t)\Delta\tau\\ \varepsilon_{\mathrm{gt}}(0)=0\\ \varepsilon_{\mathrm{gl}}(0)=0\end{cases}. \tag{25}$$

Note that the growth strains $\varepsilon_{\mathrm{gt}}$ and $\varepsilon_{\mathrm{gl}}$ in the oxide are assumed to be independent of the *z*-axis coordinate and uniform throughout the thickness, due to the very small thickness of the oxide scale.

2.6 Implementation of the semi-analytical method

The semi-analytical method is implemented in a Fortran code. The procedures of the method are shown in Fig. 4, in which the iterative approach is used to calculate the stress evolution during the thermal cycling. The main steps of the implementation are summarized as below:

- *Step 0*: Initiate the coating system. The creep strain, TGO growth strain, total strain, and stresses in the system are defined as zero, namely $\varepsilon_{\mathrm{c}}(z,0)=0$, $\varepsilon_{\mathrm{gt}}(0)=0$, $\varepsilon_{\mathrm{gl}}(0)=0$, $\varepsilon(z,0)=0$, and $\sigma(z,0)=0$;
- *Step 1*: Impose a time increment Δt;
- *Step* 2: Determine the temperature field $T(z, t)$ using Eq.(3);
- *Step 3*: Determine the creep strain field $\varepsilon_{\mathrm{c}}(z,t)$ using Eqs.(19) and (20);

- *Step 4*: Calculate the TGO growth strain $\varepsilon_{gt}(t)$ and $\varepsilon_{gl}(t)$ using Eqs.(23), (24) and (25);
- *Step 5*: Calculate the $c(t)$, $t_b(t)$, and $r(t)$ using Eqs.(10), (11) and (12). Then, the total strain field $\varepsilon(z,t)$ is obtained by Eq.(4);
- *Step 6*: Calculate the stress field by Eq.(5);
- *Step 7*: If it is the end of the analysis, move to Step 1. Otherwise, the analysis is finished.

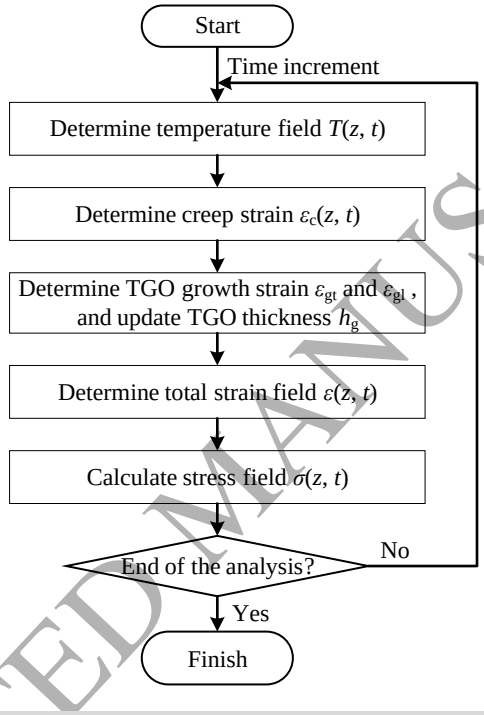

Fig. 4. Flowchart of the semi-analytical method

3. Verification by finite element analysis

To verify the validity of the proposed semi-analytical model, a finite element analysis (FEA) of the TBCs is carried out in ABAQUS and comparisons of the stress and inelastic strain fields are made with the semi-analytical solutions.

3.1 Finite element analysis

As shown in Fig. 5(a), the TBCs is composed of four components: two layers of ceramic coatings (coating1 and coating2), a layer of oxide scale (known as thermally grown oxide, TGO), and a substrate. The material properties are listed in Table 1, in which the Poisson's

ACCEPTED MANUSCRIPT

ratios are also given. In the semi-analytical model, the role of the Poisson's ratio is to transform the Young's modulus E^* of a layer into the biaxial modulus E (namely $E= E^*/(1-\nu)$). In addition to that, the Poisson's ratio in FEA acts as an essential material parameter in constructing the stiffness matrix for the finite elements.

Ten thermal cycles are imposed in the analyses. Each single cycle includes 5 min heating, 10 h high-temperature holding, and then 5 min cooling, as illustrated in Fig. 5(c). The system is initially stress-free at 20℃. During the high-temperature holding period, the imposed temperature at the top surface and bottom surface of the model are 1400℃ and 950℃, respectively, such that a gradient of 450℃ is formed across the entire system.

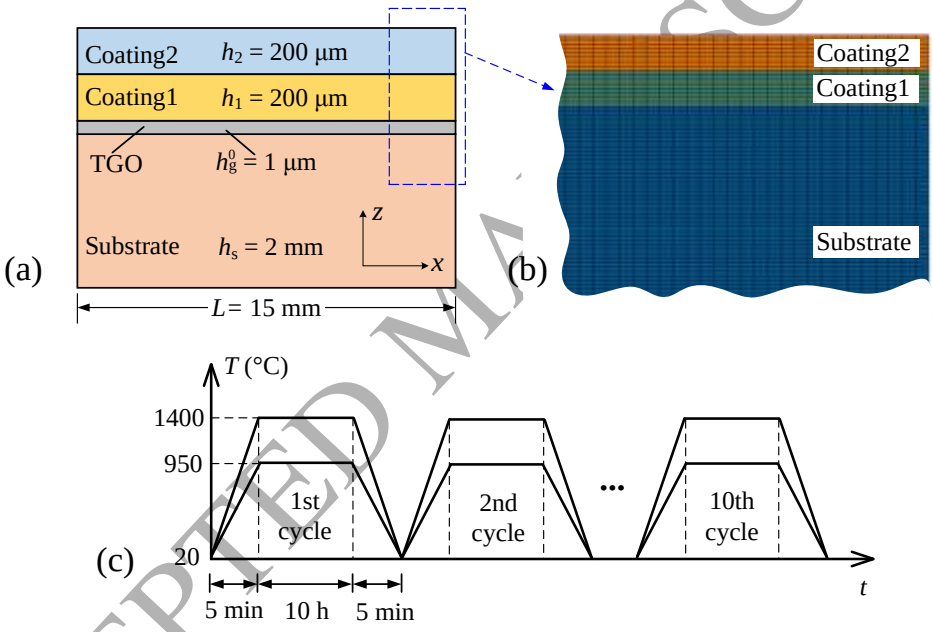

Fig. 5. Schematic showing: (a) geometry of the finite element model, (b) FE meshes, and (c) thermal loading history.

Table 1. Material properties of the TBCs layers [21, 35, 36].

Layer	Young's modulus (GPa)	Poisson's ratio	Thermal conductivity ($W\cdot(m\cdot℃)^{-1}$)	Thermal expansion ($\times10^{-6}$ $℃^{-1}$)	Creep prefactor ($MPa^{-n}\cdot s^{-1}$)	Creep exponent
Coating2	60	0.25	0.81	8.2	5.0×10^{-10}	1
Coating1	48	0.1	1.88	9.0	5.0×10^{-10}	1
TGO	400	0.23	23.0	8.0	5.0×10^{-10}	1
Substrate	184	0.3	30.0	16.0	5.0×10^{-10}	1

The FE model is meshed with two-dimensional 8-node biquadratic element, the type of

which are DC2D8 in thermal analysis and CPS8R in stress analysis. The nominal mesh size in the thickness direction and length direction are 0.025 mm and 0.075 mm, respectively, as shown in Fig. 5(b). Four layers of elements are contained in the TGO layer to accurately calculate the stresses along its thickness direction. The total element numbers of the FE model are 20000. The mesh sensitivity study has been performed and revealed that the meshes are sufficient to achieve the mesh size independent results.

In the FE simulations, the sequentially-coupled method is used to analyze the stress fields. This method considers that the stress fields depend on the temperature fields, but the reverse is not significant. In the mechanical analysis, the symmetric boundary condition is applied on the left edge of the model, and the node at bottom of this edge is fixed to constrain the movement of the model along the *z*-axis direction. The SLIDER type multiple point constraint (MPC) in ABAQUS is set on the right edge to keep the nodes on it to deform and move along a straight line, which is used to model the infinite-length system.

Table 2. Parameters of oxidation growth kinetics.

k_{op} (μm^2/h)	Q (kJ/mol)	R (J/(mol·K))	m_g	η_g
3.15×10^6	206.273	8.314472	1/2	0.1

Note: The k_{op} and η_g are selected in this work, and other parameters are taken from literature [37].

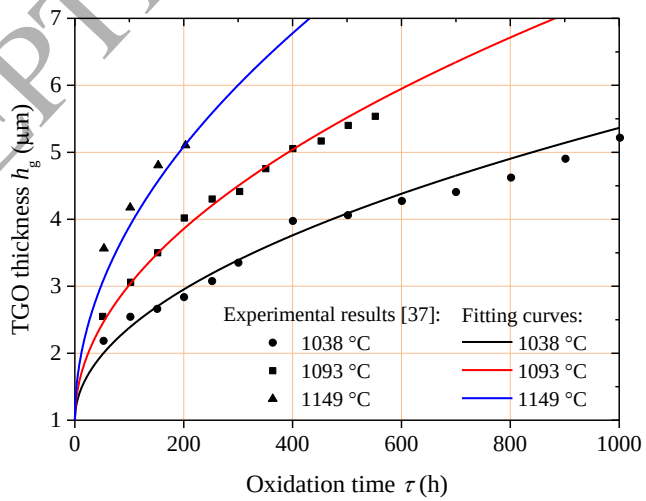

Fig. 6. Temperature-dependent oxide growth kinetics

The oxide growth is simulated in the FEA by considering all the TGO elements swell

both in the thickness direction and the lateral direction (via the subroutine UEXPAN in ABAQUS). The parameters of the oxide growth kinetics are listed in Table 2, in which the parameter k_{op} is fitted in this work. Fig. 6 shows the experimentally measured temperature-dependent kinetics (taken from [37]) and the corresponding fitting curves using the parameters in Table 2. The comparisons indicate that the selected k_{op} works quite well.

3.2 Comparison between FEA and semi-analytical predictions

The temperature distribution in the *z*-direction is shown in Fig. 7. The analytical results are consistent with the FEA predictions. Ceramic coatings provide a total of 379℃ thermal insulation. The temperature gradient in the coating2 is greater than the one in the coating1 due to the lower thermal conductivity of the former layer.

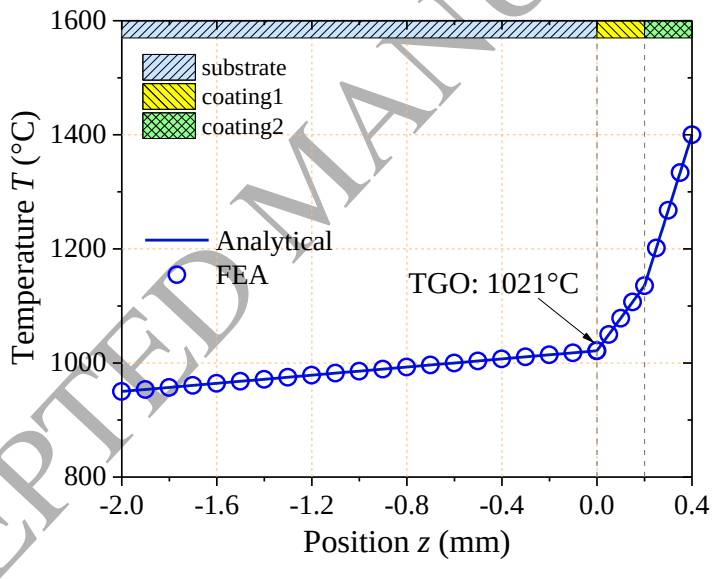

Fig. 7. Comparison between the FEA and analytical prediction: temperature distribution in the through-thickness direction.

The stress contours (σ_x) taken from the FEA at different instants of the thermal cycles are shown in Fig. 8, in which the results of TGO layer are excluded due to its much higher stresses than the other layers. It is observed that the stresses at the high-temperature period are relaxed (Fig. 8(a, b, d)), whereas the residual stresses at the ambient temperature are enhanced with the thermal cycles (Fig. 8(c, e)). Simultaneously, the curvature of the system is seen to vary with the thermal cycles. After heating from the initially stress-free state in the first cycle,

ACCEPTED MANUSCRIPT

the coating system bends upward to form the concave shape (corresponds to negative 1/*r*). Due to the creep relaxations in the system, the curvature enhances with the high-temperature exposure time, and significant residual deformations remain after the system is cooled down.

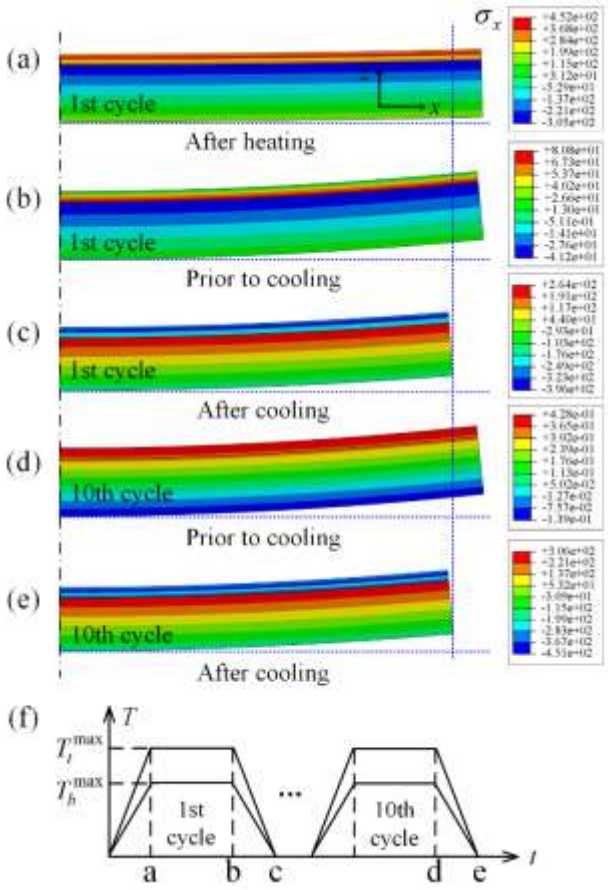

Fig. 8. FE predictions of stress contours σ_x at different instants: (a) after heating in the 1st cycle; (b) prior to cooling in the 1st cycle; (c) after cooling in the 1st cycle; (d) prior to cooling in the 10th cycle; (e) after cooling in the 10th cycle; (f) schematic showing the above five instants in the thermal loading history. (The deformations are magnified by a factor of 5, and TGO layer is excluded from the contours).

The quantitative evolution of the curvature is plotted in Fig. 9. Due to the difficulty in deriving the curvature from the finite element model, only the result of the semi-analytical method is presented. After the second thermal cycle, the evolution of the curvature tends to be stable because the stresses in the coatings and substrate are nearly relaxed to zero from then on, as will be seen in Fig. 12. In particular, it is observed that the increment of the curvature in the heating stage is opposite to the one in the cooling stage, due to the imposed opposite thermal loads. For instance, heating in first thermal cycle induces the negative increment of

1/*r* to form the concave curvature, whereas cooling in the following cycles gives rise to the positive increment of 1/*r* to alleviate the concave curvature. The phenomenon of opposite increment of curvature between the heating and cooling stages is helpful in understanding the variation of curvature during the thermal cycling, especially in the case when the curvature reversal occurs (as will be seen in Section 4).

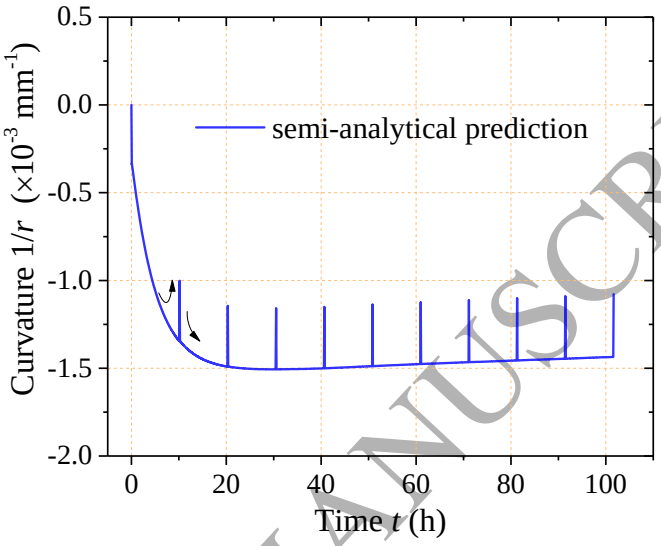

Fig. 9. Evolutions of curvature of the system predicted by semi-analytical model

The stress and creep strain distributions in the through-thickness direction at different instants of the thermal cycles are plotted in Fig. 10 and Fig. 11, in which comparisons are made between the semi-analytical and FEA predictions. Generally, the results determined by the semi-analytical method correlate well with the FEA, which confirms the validity of the proposed model. Stresses and creep strains are linearly distributed in an individual layer. After initially heating in the first cycle, the coating layers are under tension due to their low CTEs, and the upper and lower sides of the substrate are under compression and tension, respectively. During the high-temperature period, stresses are relaxed to reach the nearly stress-free state (e.g., in the case of prior to cooling in the 10th cycle), but the creep strains accumulate instead. Simultaneously, the residual stresses are enhanced with the thermal cycles, as seen in Fig. 10(b). It is interesting that the stress distributions at the first heating state (the case of after heating in the 1st cycle) and final cooling state (the case of after cooling in the 10th cycle)

ACCEPTED MANUSCRIPT

have the same magnitude but the opposite sign. It results from the imposed opposite thermal loads on the stress-free system. This phenomenon suggests that design of the coatings system should account for the thermal stresses at the high-temperature state as well as the residual stresses at the ambient temperature state because these stresses with opposite sign would affect the durability of the coatings in different manners.

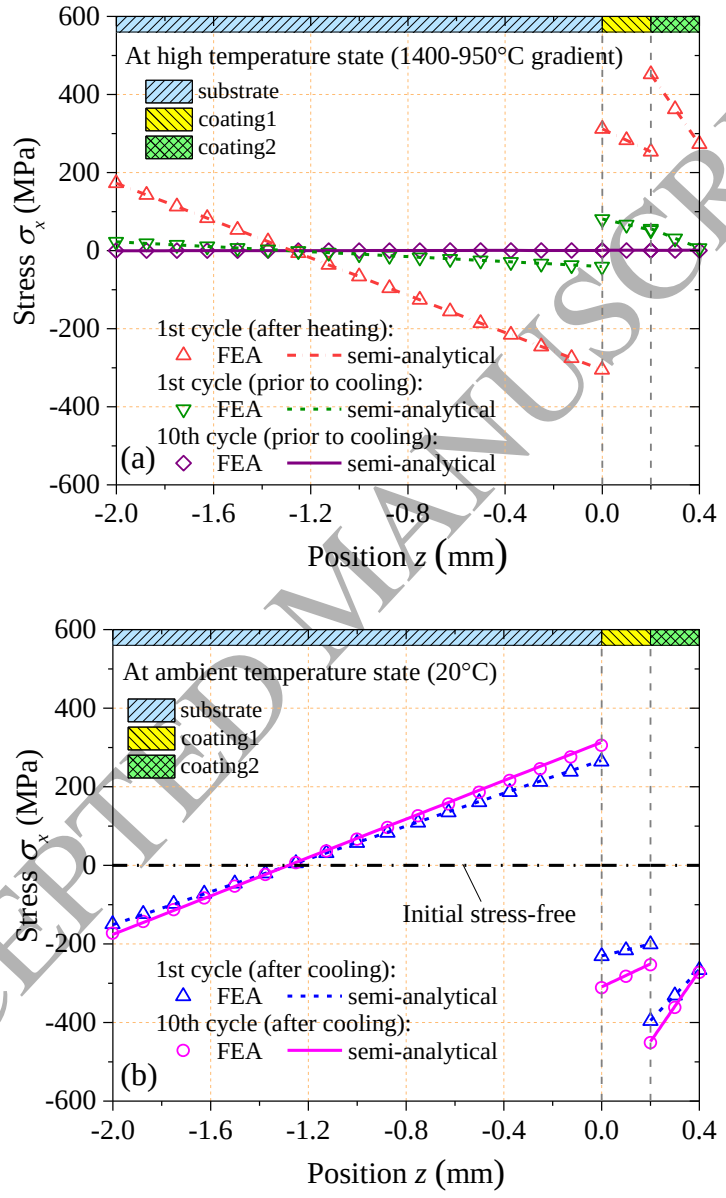

Fig. 10. Comparisons between the FEA and semi-analytical predictions: stress distributions in the through-thickness direction at (a) high-temperature states and (b) ambient temperature states (the results of TGO are excluded).

ACCEPTED MANUSCRIPT

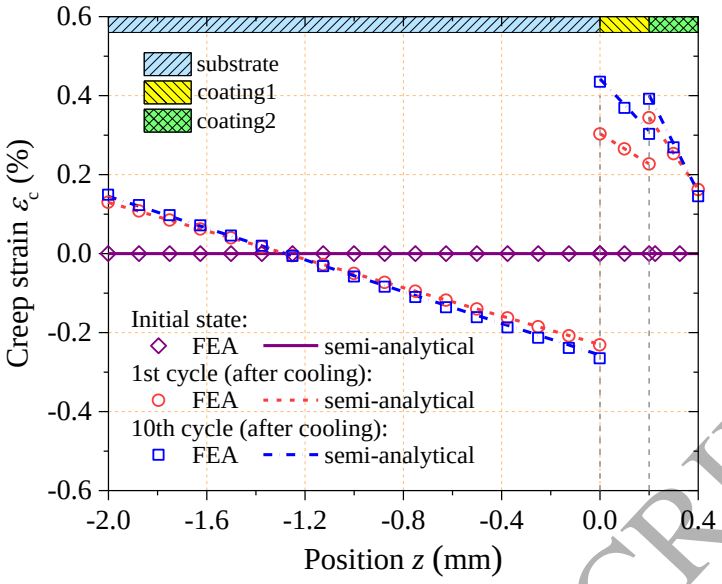

Fig. 11. Comparisons between the FEA and semi-analytical predictions: creep strain distributions at cooling states of the 1st and 10th cycles (the results of TGO are excluded).

Fig. 12 presents the evolutions of stresses and creep strains at three representative positions. Again, the semi-analytical solutions are consistent with the FEA predictions. As the high-temperature exposure time extends, the creep strains at the locations of $z = 0.2^+$ and -2 almost stop to accumulate after the thermal stresses are relaxed to zero (from the 3rd cycle). However, as seen in Fig. 12(f), the creep strain in TGO continuously accumulates till the end of the thermal loading history. It results from the relaxations of continuously rising growth stresses caused by the lateral growth of TGO. During the cycling, some balance is formed between the growth stresses and creep relaxation so that the stress evolution in TGO tends to be stable (Fig. 12(e)).

ACCEPTED MANUSCRIPT

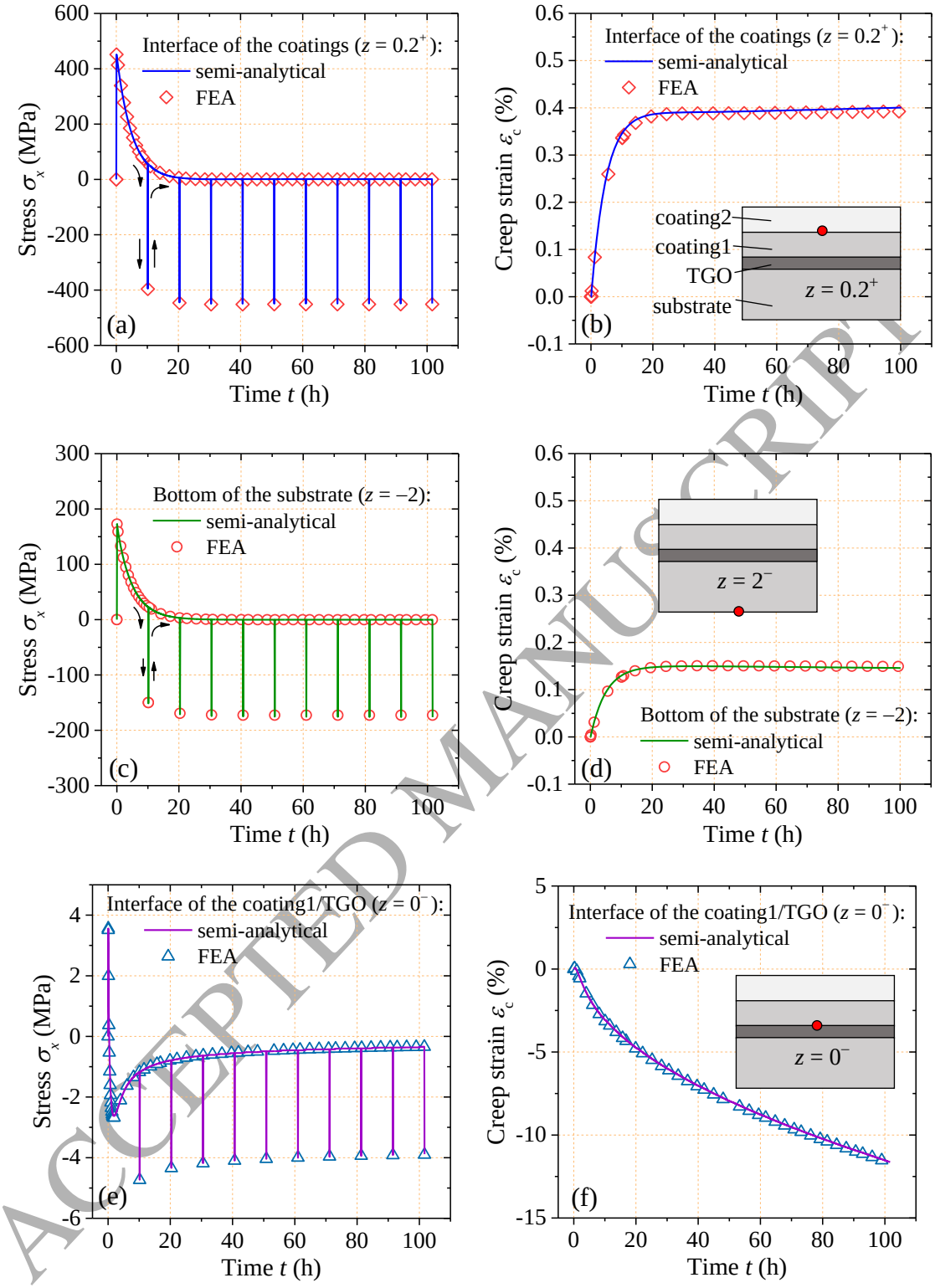

Fig. 12. Comparison between the FEA and semi-analytical predictions: (a, c, e) stress evolutions and (b, d, f) creep strain evolutions at the (a, b) interface of the coatings, (c, d) bottom of the substrate, and (e, f) interface of the coating1/TGO ($z = 0.2^+$ denotes that the position is adjacent to the interface on the coating2 side, and $z = 0^-$ denotes that it is on the TGO side).

4. Results and discussions

Creep deformations in the multilayer coating system may significantly affect the stress evolutions during the thermal cycling, so as to alter the features of curvature of the system. By using the proposed semi-analytical method, the effects of creep in the substrate, coatings, and TGO on the stress evolutions are respectively studied. In these analyses, except for discussions on various creep prefactors, the material properties in Tables 1 and 2 are selected as the benchmark cases. The geometries of the system are the same with that used in Section 3 (see Fig. 5). For ease of presentation and comparison, a single full cycle with a long holding time is employed in this section, which includes 5 min heating, 100 h high-temperature holding, and then 5 min cooling.

4.1 Effect of creep in substrate

The creep prefactors B_s are assumed to range from zero to 5×10^{-9} to illustrate the effect of creep in the substrate. The $B_s = 0$ is used to model the elastic substrate without creep deformation, and $B_s = 5\times10^{-11}$, 5×10^{-10} and 5×10^{-9} are adopted to represent the viscoelastic substrate with low, medium and fast creep rates, respectively.

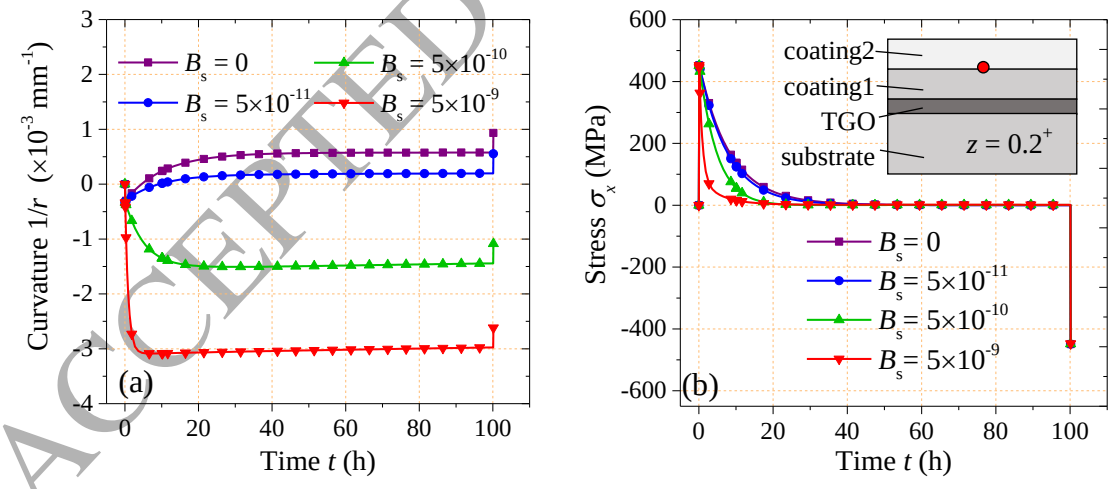

ACCEPTED MANUSCRIPT

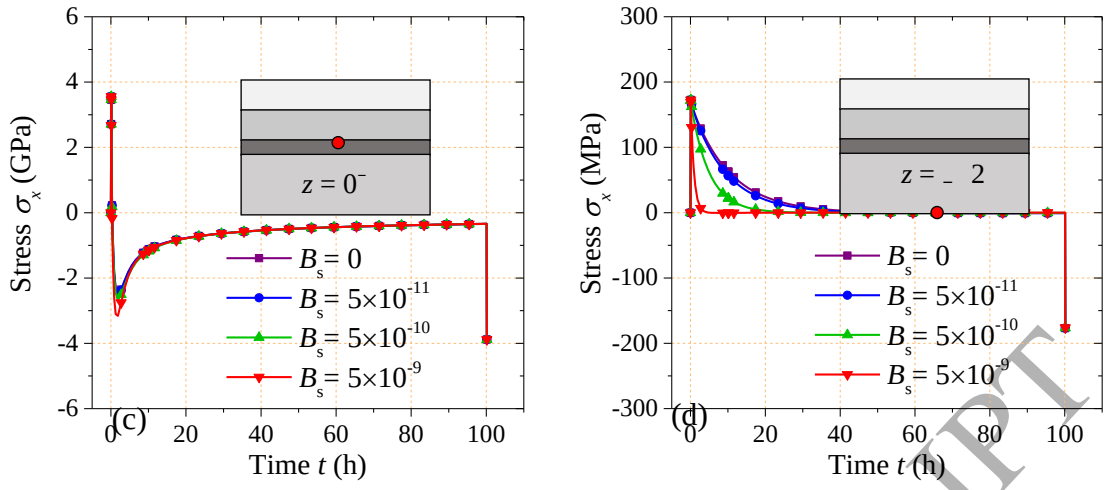

Fig. 13. Effect of creep in the substrate: (a) evolutions of curvature of the system; and stress evolutions at (b) coating1/coating2 interface (on the coating2 side); (c) coating1/TGO interface (on TGO side); (d) bottom of the substrate.

The evolutions of curvature of the system are shown in Fig. 13 (a). Creep rates in the substrate strongly affect the curvature evolutions. For the substrate with elastic or slow creep behaviors, the curvature reverses from concave to the convex shape as the holding time increases. However, the curvature remains as the concave shape for the medium and fast creep substrate, in which the larger B_s gives rise to the larger curvature. Regardless of the various creep behaviors in the coatings, the cooling process tends to induce the system bending downward. Therefore, no matter whether the curvature reversal occurs or not, the cooling processes in all the cases induce the positive increment of $1/r$, leading to the enhancement of convex curvature for small B_s and the decrease of concave curvature for large B_s.

The stress evolutions at three locations in the system are presented in Fig. 13 (b)-(d). In general, stress relaxation processes in the coatings and substrate are facilitated by the faster creep of the substrate. However, stress evolutions in the TGO are almost unaffected by the B_s. The so-called 'stress shift' occurs in TGO, which is the shift of stresses from tensile to compressive during the holding period [38]. This phenomenon results from the competitions among thermal expansion mismatch, oxidation growth, and creep relaxation. After the system is heated up, the stress in TGO is in tension due to its lower CTE than the substrate. As the

ACCEPTED MANUSCRIPT

holding time increases, the lateral growth of TGO induces the compressive growth stress so that the stress shifts to compressive state. In the same process, creep deformations gradually relax such growth stresses to approach zero.

4.2 Effect of creep in coatings

The creep prefactors of the coating1 and coating2 are assumed to be identical ($B_1 = B_2 = B_c$) and they are set to range from zero to 5×10^{-9} to study the effect of creep in the coatings. The curvature evolutions under various B_c are shown in Fig. 14(a). Coatings with fast creep rates induce the reversal of curvature from concave to the convex shape, whereas the slow creep coatings give rise to the enhancement of concave curvature. Fig. 14 (b)-(d) show the stress evolutions at the three locations in the system. The large B_c leads to the fast stress relaxations in the coatings as well as the substrate. But the stresses in TGO is virtually unaffected. These findings are consistent with the discussions of B_s given in Section 4.1.

Above observations suggest that variations of curvature of the system are determined by the comparisons between the creep rates in the substrate and the coatings. For the case of 'fast creep substrate + elastic/slow creep coatings', as shown in Fig. 15, the substrate quickly loses the resistance to bending when exposed to the high temperature. In the same process, however, stresses in the coatings are unable to be fully relaxed by creep deformations. In order to ensure the equilibrium of the force and moment in the system, the concave curvature is enhanced to increase the negative bending strains in the coatings so that the tensile stresses in the coatings are able to be reduced. In contrast, for the case of 'elastic/slow creep substrate + fast creep coatings', significant stresses remain in the substrate after the coatings are relaxed to become the stress-free. Thus, the curvature has to reverse from the concave to the convex shape to change the signs of bending strains in the substrate, such that stresses within it could be reduced to achieve the system equilibrium.

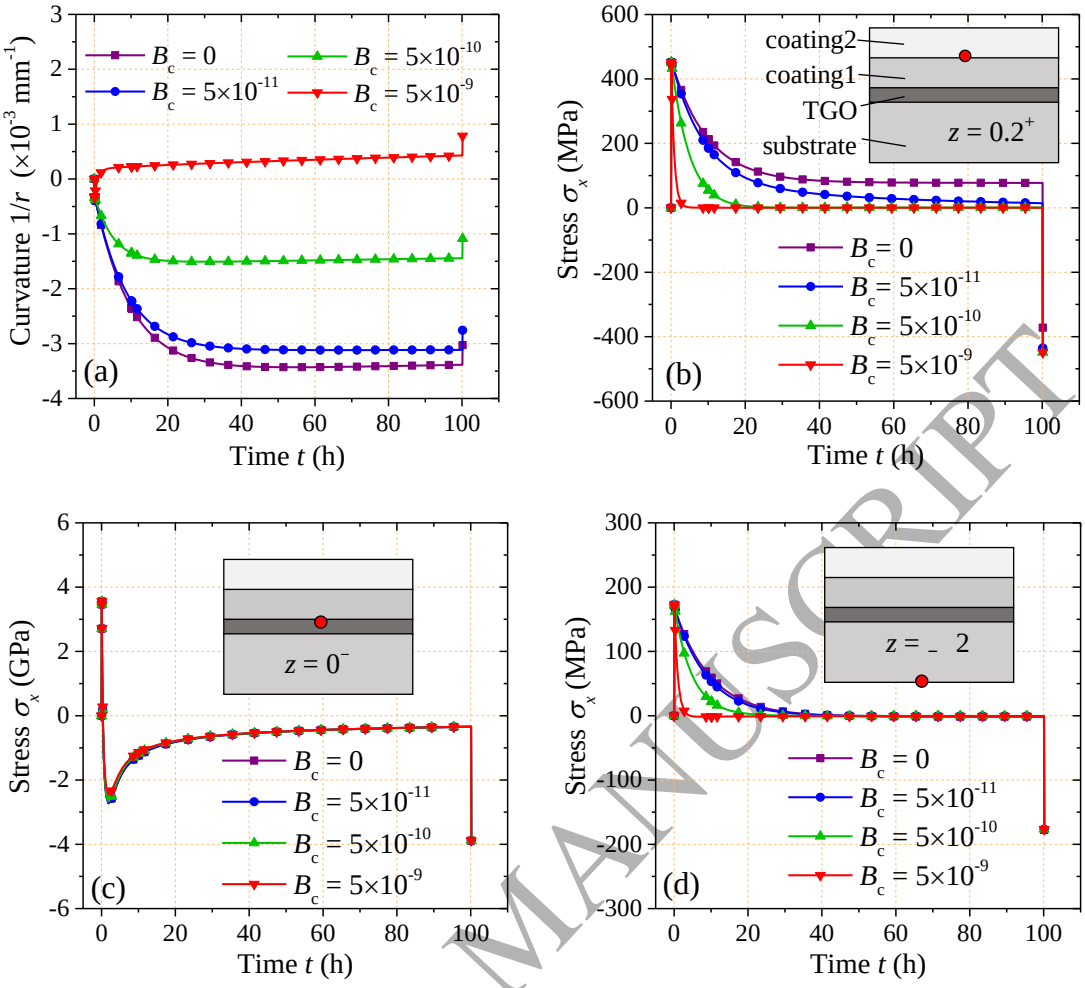

Fig. 14. Effect of creep in the coatings: (a) evolutions of curvature of the system; and stress evolutions at (b) coating1/coating2 interface (on the coating2 side); (c) coating1/TGO interface (on TGO side); (d) bottom of the substrate.

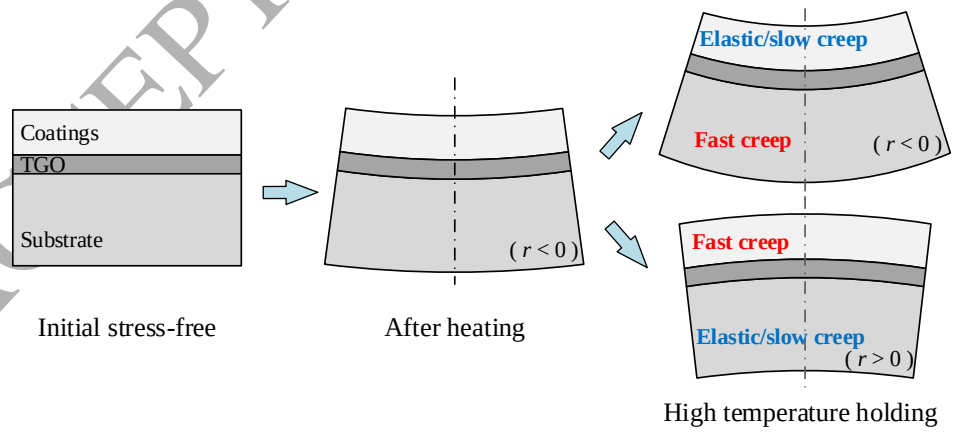

Fig. 15. Schematic diagrams showing the variations of curvature with different creep rates in the coatings and substrate.

4.3 Effect of creep in TGO

Fig. 16 shows the curvature and stress evolutions under various creep prefactor of the TGO B_g. It is seen that the creep rate in the TGO plays an important role in determining the evolutions. During the high-temperature period, the lateral growth of TGO results into the increasing of growth strains. Huge compressive growth stresses are introduced in the elastic TGO due to the constraint of the thick substrate. As the high-temperature holding time increases, the curvature of the system is reversed from concave to the convex shape and is subsequently enhanced. Such enhancement of curvature acts like resulting from an externally imposed bending moment so that the tensile and compressive stresses are developed within the coatings and at bottom of the substrate, respectively.

Nevertheless, the role of TGO becomes insignificant when its creep processes are sufficiently rapid. The fast creep relaxations in the TGO would remarkably reduce the growth stresses, such that the curvature and the stress fields in the system would not be affected by the TGO growth. It suggests that the competition between the growth stress generation (TGO lateral growth) and stress relaxation (creep deformation) determines the features of the evolutions. The dominant of growth stress generation is disadvantageous to the reliability of the system because the stresses in the system may gradually evolve to a high level. Appropriate creep deformations in TGO provide benefits in relaxing huge growth stress so that the better durability of the system could be obtained.

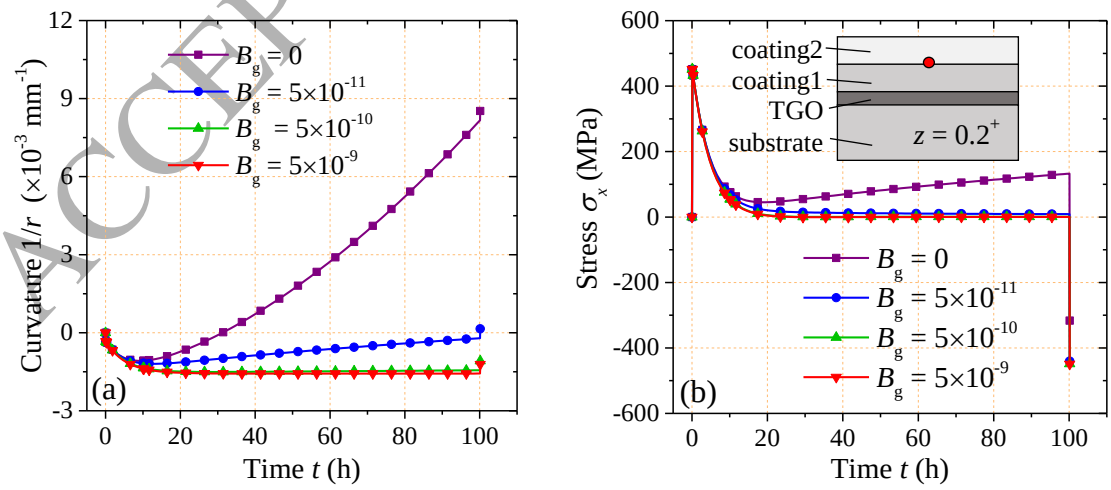

ACCEPTED MANUSCRIPT

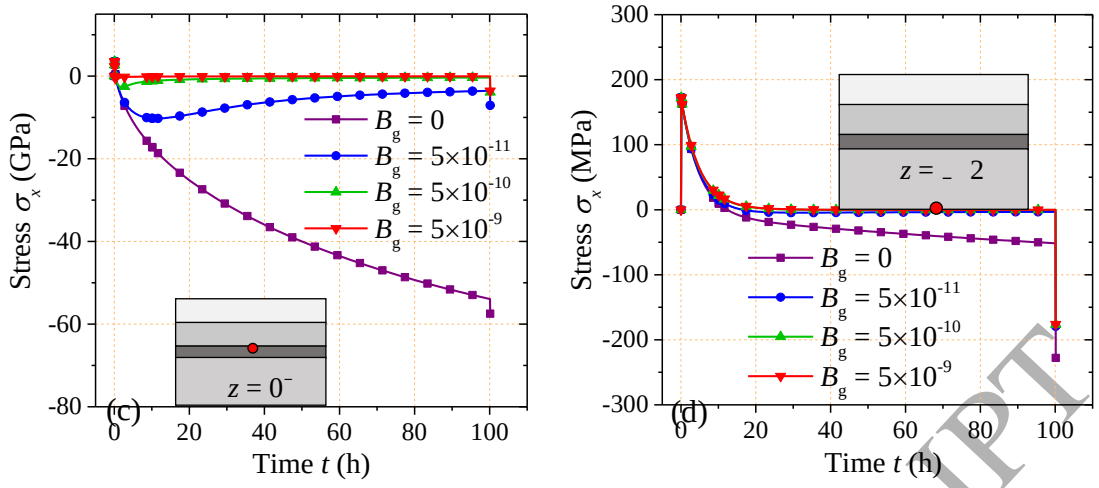

Fig. 16. Effect of creep in the TGO: (a) evolutions of curvature of the system; and stress evolutions at (b) coating1/coating2 interface (on the coating2 side); (c) coating1/TGO interface (on TGO side); (d) bottom of the substrate.

5. Conclusion

A semi-analytical model is developed to estimate the stress evolution in a multilayer coating system during cyclic thermal loading. The thermal gradient conditions, oxide scale growth, and creep relaxation processes are taken into account in the model. The oxide growth kinetics is introduced to determine the oxide thickness as well as the lateral growth strains. During the thermal cycling, the temperature and stress fields are solved by the iterative approach, in which the numerical method is used to calculate the integrations related to the time-dependent creep strains.

Specific analyses were made for the thermal barrier coatings with double ceramic layers. The proposed model is validated by the comparisons of stress and creep strain fields between the semi-analytical and finite element predictions. The creep rates in the layers significantly affect the evolutions of stresses as well as curvature of the system. Large creep rates in the coatings or substrate could facilitate the stress relaxations in both of them, whereas the stress evolutions in the TGO are virtually unaffected. As the holding time increases, the curvature would reverse from concave to convex shape for the case of ‘elastic/slow creep substrate + fast creep coatings’, whereas the concave curvature remains and enhances for the case of ‘fast creep substrate + elastic/slow creep coatings’. Furthermore, the competition between the

ACCEPTED MANUSCRIPT

lateral growth and creep deformation in the oxide scale determines the features of the stress evolutions. The creep deformations in the oxide provide benefits in relaxing the huge growth stresses so that the better durability of the system could be obtained.

Acknowledgements

This work is supported by China 973 Program (2013CB035700) and National Natural Science Foundation of China (11472204 and 11602188).

Appendix A. Determination of the uniform strain component

The integration related to the temperature gradient $\Delta T(z,t)$ in the uniform strain component (Eq. (10)) is written as follows:

$$\int_{-(h_s+h_g)}^{z_n} E(z)\alpha(z)\Delta T(z,t)\mathrm{d}z = E_s\alpha_s\int_{-(h_s+h_g)}^{-h_g}\Delta T(z,t)\mathrm{d}z + E_g\alpha_g\int_{-h_g}^{0}\Delta T(z,t)\mathrm{d}z + \sum_{i=1}^{n}E_i\alpha_i\int_{z_{i-1}}^{z_i}\Delta T(z,t)\mathrm{d}z, \quad \text{(A-1)}$$

where

$$\int_{-(h_s+h_g)}^{-h_g}\Delta T(z,t)dz = \left[p_1 - p_2\left(\sum_{i=1}^{n}\frac{h_i}{\lambda_i} + \frac{h_g}{\lambda_g} - \frac{h_g}{\lambda_s}\right)\right]h_s + \frac{p_2}{2\lambda_s}\left[{h_g}^2 - \left(h_s+h_g\right)^2\right], \quad \text{(A-2)}$$

$$\int_{-h_g}^{0}\Delta T(z,t)\mathrm{d}z = \left(p_1 - p_2\sum_{i=1}^{n}\frac{h_i}{\lambda_i}\right)h_g - \frac{p_2}{2\lambda_g}{h_g}^2, \quad \text{(A-3)}$$

$$\int_{z_{i-1}}^{z_i}\Delta T(z,t)\mathrm{d}z = \left[p_1 - p_2\left(\sum_{j=i+1}^{n}\frac{h_j}{\lambda_j} + \frac{z_i}{\lambda_i}\right)\right]h_i + \frac{p_2}{2\lambda_i}\left({z_i}^2 - {z_{i-1}}^2\right), \quad \text{(A-4)}$$

$$p_1 = T_t(t) - T_0, \quad p_2 = \frac{T_t(t) - T_b(t)}{R_{\text{total}}}. \quad \text{(A-5)}$$

The integration related to the creep strain in Eq. (10) is written as follows:

$$\int_{-(h_s+h_g)}^{z_n} E(z)\varepsilon_c(z,t)\mathrm{d}z = E_s\int_{-(h_s+h_g)}^{-h_g}\varepsilon_c(z,t)\mathrm{d}z + E_g\int_{-h_g}^{0}\varepsilon_c(z,t)\mathrm{d}z + \sum_{i=1}^{n}E_i\int_{z_{i-1}}^{z_i}\varepsilon_c(z,t)\mathrm{d}z. \quad \text{(A-6)}$$

Due to the difficulty in deriving the closed-form integrations of time-dependent creep

strains, the compound Cotes integration formulation is used to numerically calculate the integrations in Eq. (A-6).

Appendix B. Determination of the radius of curvature *r*(*t*)

The integration related to the temperature gradient in Eq. (18) is written as follows:

$$\begin{aligned}\int_{-(h_s+h_g)}^{z_n} E(z)\alpha(z)\Delta T(z,t)\left[z-t_b(t)\right]\mathrm{d}z = -t_b(t)\int_{-(h_s+h_g)}^{z_n} E(z)\alpha(z)\Delta T(z,t)\mathrm{d}z + \\ E_s\alpha_s\int_{-(h_s+h_g)}^{-h_g} z\Delta T(z,t)\mathrm{d}z + E_g\alpha_g\int_{-h_g}^{0} z\Delta T(z,t)\mathrm{d}z + \sum_{i=1}^{n} E_i\alpha_i\int_{z_{i-1}}^{z_i} z\Delta T(z,t)\mathrm{d}z\end{aligned}, \tag{B-1}$$

where

$$\int_{-(h_s+h_g)}^{-h_g} z\Delta T(z,t)\mathrm{d}z = \left[p_1 - p_2\left(\sum_{i=1}^{n}\frac{h_i}{\lambda_i} + \frac{h_g}{\lambda_g} - \frac{h_g}{\lambda_s}\right)\right]\frac{h_g^{\,2} - (h_s+h_g)^2}{2} + \frac{p_2}{\lambda_s}\frac{(h_s+h_g)^3 - h_g^{\,3}}{3}, \tag{B-2}$$

$$\int_{-h_g}^{0} z\Delta T(z,t)\mathrm{d}z = \left(p_1 - p_2\sum_{i=1}^{n}\frac{h_i}{\lambda_i}\right)\frac{-h_g^{\,2}}{2} + \frac{p_2}{\lambda_g}\frac{h_g^{\,3}}{3}, \tag{B-3}$$

$$\int_{z_{i-1}}^{z_i} z\Delta T(z,t)\mathrm{d}z = \left[p_1 - p_2\left(\sum_{j=i+1}^{n}\frac{h_j}{\lambda_j} + \frac{z_i}{\lambda_i}\right)\right]\frac{z_i^{\,2} - z_{i-1}^{\,2}}{2} + \frac{p_2}{\lambda_i}\frac{z_i^{\,3} - z_{i-1}^{\,3}}{3}. \tag{B-4}$$

In the Eqs. (B-2)~(B-4), the coefficients p_1 and p_2 are taken from the Eq. (A-5). The integration related to the creep strain is written as follows:

$$\begin{aligned}\int_{-(h_s+h_g)}^{z_n} E(z)\varepsilon_c(z,t)\left[z-t_b(t)\right]\mathrm{d}z = E_s\int_{-(h_s+h_g)}^{-h_g}\varepsilon_c(z,t)\left[z-t_b(t)\right]\mathrm{d}z \\ +E_g\int_{-h_g}^{0}\varepsilon_c(z,t)\left[z-t_b(t)\right]\mathrm{d}z + \sum_{i=1}^{n}E_i\int_{z_{i-1}}^{z_i} z\varepsilon_{cr}(z,t)\left[z-t_b(t)\right]\mathrm{d}z\end{aligned}. \tag{B-5}$$

Similar to the Eq. (A-6), the Eq. (B-5) is also numerically solved by the compound Cotes integration formulation.

References

[1] M. Guler, Y. Alinia, S. Adibnazari, On the rolling contact problem of two elastic solids with graded coatings, International Journal of Mechanical Sciences, 64 (2012) 62-81.
[2] T.P. Gotkhindi, K. Simha, Transverse elastic response of bundled coated cylinders, International Journal of Mechanical Sciences, 76 (2013) 70-85.
[3] R. Kulchytsky-Zhyhailo, A.S. Bajkowski, Axisymmetrical problem of thermoelasticity for

ACCEPTED MANUSCRIPT

ACCEPTED MANUSCRIPT

halfspace with gradient coating, International Journal of Mechanical Sciences, 106 (2016) 62-71.
[4] N.P. Padture, M. Gell, E.H. Jordan, Thermal barrier coatings for gas-turbine engine applications, Science, 296 (2002) 280-284.
[5] R. Xu, X. Fan, T. Wang, Mechanisms governing the interfacial delamination of thermal barrier coating system with double ceramic layers, Applied Surface Science, 370 (2016) 394-402.
[6] J.G. Lim, S. Seo, J.M. Koo, C.S. Seok, J.B. Choi, M.K. Kim, Parametric study for optimal design of an air plasma sprayed thermal barrier coating system with respect to thermal stress, Surface and Coatings Technology, 315 (2017) 105-111.
[7] Y. Lu, L. Luo, J. Liu, C. Zhu, Y. Wang, Failure Mechanism Associated with the Thermally Grown Silica Scale in Environmental Barrier Coated C/SiC Composites, Journal of the American Ceramic Society, 99 (2016) 2713-2719.
[8] E. Bakan, D. Marcano, D. Zhou, Y.J. Sohn, G. Mauer, R. Vaßen, Yb2Si2O7 Environmental Barrier Coatings Deposited by Various Thermal Spray Techniques: A Preliminary Comparative Study, Journal of Thermal Spray Technology, (2017) 1-14.
[9] B.T. Richards, S. Sehr, F. de Franqueville, M.R. Begley, H.N. Wadley, Fracture mechanisms of ytterbium monosilicate environmental barrier coatings during cyclic thermal exposure, Acta Materialia, 103 (2016) 448-460.
[10] S. Faulhaber, C. Mercer, M.-W. Moon, J. Hutchinson, A. Evans, Buckling delamination in compressed multilayers on curved substrates with accompanying ridge cracks, Journal of the Mechanics and Physics of Solids, 54 (2006) 1004-1028.
[11] D.G. Ninh, D.H. Bich, Nonlinear buckling of eccentrically stiffened functionally graded toroidal shell segments under torsional load surrounded by elastic foundation in thermal environment, Mechanics Research Communications, 72 (2016) 1-15.
[12] B. Li, Y. Li, J. Su, A combined interface element to simulate interfacial fracture of laminated shell structures, Composites Part B: Engineering, 58 (2014) 217-227.
[13] T. Qasim, M.B. Bush, X.-Z. Hu, The influence of complex surface geometry on contact damage in curved brittle coatings, International journal of mechanical sciences, 48 (2006) 244-248.
[14] J. Zhuang, Z. Xiao, Generalized Irwin plastic zone correction of a sub-interface Zener–Stroh crack in a coating-substrate system, International Journal of Mechanical Sciences, 94 (2015) 123-130.
[15] H.J. Choi, Interfacial fracture analysis of bonded dissimilar strips with a functionally graded interlayer under antiplane deformation, Mechanics Research Communications, (2015).
[16] Y. Sun, J. Li, W. Zhang, T. Wang, Local stress evolution in thermal barrier coating system during isothermal growth of irregular oxide layer, Surface and Coatings Technology, 216 (2013) 237-250.
[17] W. Mao, Y. Zhou, L. Yang, X. Yu, Modeling of residual stresses variation with thermal cycling in thermal barrier coatings, Mechanics of materials, 38 (2006) 1118-1127.
[18] O.M. Abuzeid, H.S. Alkhaldi, P. Eberhard, A thermal creep model for the contact of nominally flat surfaces: Jeffreys' linear visco-elastic model, International Journal of Mechanical Sciences, 53 (2011) 910-917.
[19] A.G. Evans, D. Mumm, J. Hutchinson, G. Meier, F. Pettit, Mechanisms controlling the durability of thermal barrier coatings, Progress in materials science, 46 (2001) 505-553.
[20] M. Thouless, J. Gupta, J. Harper, Stress development and relaxation in copper films during thermal cycling, Journal of materials research, 8 (1993) 1845-1852.
[21] G. Di Girolamo, F. Marra, M. Schioppa, C. Blasi, G. Pulci, T. Valente, Evolution of microstructural and mechanical properties of lanthanum zirconate thermal barrier coatings at high temperature, Surface and Coatings Technology, 268 (2015) 298-302.
[22] M.G. Gok, G. Goller, Production and characterisation of GZ/CYSZ alternative thermal barrier coatings with multilayered and functionally graded designs, Journal of the European Ceramic Society, 36 (2016) 1755-1764.
[23] G. Janssen, M. Abdalla, F. Van Keulen, B. Pujada, B. Van Venrooy, Celebrating the 100th anniversary of the Stoney equation for film stress: Developments from polycrystalline steel strips to single crystal silicon wafers, Thin Solid Films, 517 (2009) 1858-1867.
[24] S. Timoshenko, Analysis of bi-metal thermostats, JOSA, 11 (1925) 233-255.
[25] V. Teixeira, Mechanical integrity in PVD coatings due to the presence of residual stresses, Thin Solid Films, 392 (2001) 276-281.
[26] C. Hsueh, Thermal stresses in elastic multilayer systems, Thin solid films, 418 (2002) 182-188.
[27] C. Hsueh, A. Evans, Residual stresses in meta/ceramic bonded strips, Journal of the American Ceramic Society, 68 (1985) 241-248.
[28] X. Zhang, B. Xu, H. Wang, Y. Wu, An analytical model for predicting thermal residual stresses in multilayer coating systems, Thin Solid Films, 488 (2005) 274-282.
[29] W.M. Huang, Y.Y. Hu, L. An, Determination of stress versus strain relationship and other

ACCEPTED MANUSCRIPT

thermomechanical properties of thin films, Applied Physics Letters, 87 (2005) 201904.
[30] C. Gao, Z. Zhao, X. Li, Modeling of thermal stresses in elastic multilayer coating systems, Journal of Applied Physics, 117 (2015) 055305.
[31] C. Hsueh, C.R. Luttrell, T. Cui, Thermal stress analyses of multilayered films on substrates and cantilever beams for micro sensors and actuators, Journal of Micromechanics and Microengineering, 16 (2006) 2509-2515.
[32] Q.-Q. Chen, F.-Z. Xuan, S.-T. Tu, Modeling of creep deformation and its effect on stress distribution in multilayer systems under residual stress and external bending, Thin Solid Films, 517 (2009) 2924-2929.
[33] Q.-Q. Chen, F.-Z. Xuan, S.-T. Tu, Residual stress analysis in the film/substrate system with the effect of creep deformation, Journal of Applied Physics, 106 (2009) 033512.
[34] H.-C. Hsueh, D. Chiang, S. Lee, Modeling of relaxation of viscoelastic stresses in multi-layered thin films/substrate systems due to thermal mismatch, Thin Solid Films, 518 (2010) 7497-7500.
[35] M.T. Hernandez, A.M. Karlsson, M. Bartsch, On TGO creep and the initiation of a class of fatigue cracks in thermal barrier coatings, Surface and Coatings Technology, 203 (2009) 3549-3558.
[36] B. Li, X. Fan, K. Zhou, T. Wang, Effect of oxide growth on the stress development in double-ceramic-layer thermal barrier coatings, Ceramics International, 43 (2017) 14763-14774.
[37] S. Ahmadian, C. Thistle, E.H. Jordan, Experimental and Finite Element Study of an Air Plasma Sprayed Thermal Barrier Coating under Fixed Cycle Duration at Various Temperatures, Journal of the American Ceramic Society, 96 (2013) 3210-3217.
[38] J. Rösler, M. Bäker, K. Aufzug, A parametric study of the stress state of thermal barrier coatings: Part I: creep relaxation, Acta materialia, 52 (2004) 4809-4817.

ACCEPTED MANUSCRIPT

Graphic abstract

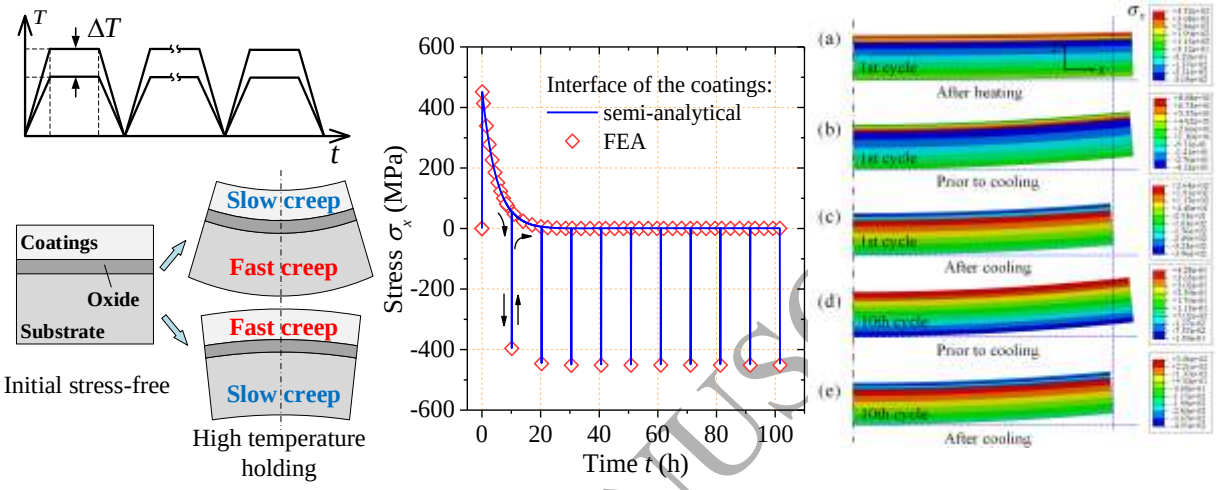

ACCEPTED MANUSCRIPT